AIAA JOURNAL
Vol. 46, No. 12, December 2008

Observation of Turbulent Mixing in Lean-Direct-Injection Combustion at Elevated Pressure

Jun Kojima*
Ohio Aerospace Institute, Cleveland, Ohio 44142
and
Quang-Viet Nguyen†
NASA John H. Glenn Research Center at Lewis Field, Cleveland, Ohio 44135

DOI: 10.2514/1.37433

We report the first quantitative single-shot multiscalar data obtained from a realistic air-fed lean-direct-injection burner operating on gaseous methane (CH_4) fuel at elevated pressure (5 atm) using single-shot spontaneous Raman spectroscopy. From a statistical analysis of the multiscalar data, we present spatially mapped probability density functions of the concentration of CH_4 and O_2, and the instantaneous temperature. The measured three-scalar correlations and probability density functions provide insights into the nature and extent of the mixing process and its impact on the subsequent combustion process. The data will also be useful for comparison with the various turbulence–chemistry interaction models such as large-eddy simulation. The swirl-stabilized flame investigated in this paper was characterized as operating in a partially premixed combustion regime that was dominated by turbulent mixing provided by the lean-direct-injection configuration. Although a majority of the single-shot data indicated complete or near-complete reactions including stoichiometric combustion, a considerable number of the data points exhibited incomplete combustion characterized by a substantial amount of residual fuel at intermediate temperatures or were simply unreacted with little or no preheating of the mixture.

I. Introduction

THE fundamental understanding of the physics and chemistry of combustion processes as well as the ability to accurately model these processes is essential to the successful development of new low-emissions combustor designs that will minimize the negative impact of aircraft engines on the local air quality and global climate. Because of the fact that the combustion process in aircraft engine combustors involves many complex thermal/fluids aspects, the numerical code development for these advanced combustors requires an increasingly sophisticated physics-based model such as large-eddy simulation (LES) [1]. Such combustion models have been applied toward turbulent combustion studies at realistic engine conditions and have attempted to capture the various aspects of aircraft engine combustion such as fuel atomization, droplet vaporization, spray-turbulence interactions, finite-rate chemical kinetics (including liquid fuels), and turbulent fuel–air mixing [2,3]. These combustion models have also been applied to simulate swirl-stabilized combustion systems (either a laboratory-scale model or realistic combustor), in which turbulence–chemistry interactions and unsteady effects of turbulent flows were highlighted [4,5].

Because of the increasing complexity of aircraft combustion systems, it is imperative that the new codes used to simulate these systems be guided and validated by careful experiment. This is the so-called code (or model) validation process [6–9]. There are several notable ongoing projects aimed at comprehensive combustion code-validation research. The Turbulent Nonpremixed Flames (TNF) Workshop is a well-known international collaboration that has made significant progress in the development of code-validation data for the computational techniques in various types of turbulent nonpremixed combustion [9,10]. The TNF Workshop's strength lies in the data provided by the one-of-the-kind facilities that are used to provide well-defined turbulent combustion experiments. In many of the experiments described by the TNF Workshops, multiple laser diagnostic methods are used to simultaneously capture major/minor species and temperature [9,10]. Many extensive studies on realistic swirl-stabilized gaseous flames at atmospheric pressure have been performed in order to develop a standardized code-validation burner [11–13]. In addition to a need for code validation with realistic burners, there is a large degree of interest in conducting such validation experiments at elevated pressures and temperatures in order to simulate actual aircraft cruise conditions. This is often challenging due to the technical challenges and safety concerns associated with pressurized systems. An example of an optically accessible, pressurized, industrial-scale research combustor has been built by the National Energy Technology Laboratory (NETL) to provide code-validation data for LES applications for natural gas-fueled, turbulent combustion [7]. This facility at NETL emphasizes research on low-emissions stationary gas-turbine combustion for power generation applications [7]. In contrast, our research focuses on the study of aircraft combustors.

In the context of aircraft engine combustion research, this paper addresses the measurement of key scalar variables critical to the analysis of turbulent mixing. Concentration measurements of the major species are an effective means for validating the different turbulence–chemistry interaction models, and even more so when combined with simultaneous temperature measurements. In particular, single-shot statistical analyses of the spatially and temporally resolved multispecies data are useful for characterizing turbulent mixing and transport processes in high-pressure flames. Temperature data in turbulent flames are also in higher demand from the standpoint of code validation, as it is intimately linked to NOx emissions generated in these engines and is critical to the determination of the combustor temperature pattern factor.

Nonintrusive laser diagnostics play a major role in the code-validation process. Coherent anti-Stokes Raman spectroscopy

Received 11 March 2008; revision received 7 July 2008; accepted for publication 9 July 2008.

*Senior Scientist, Turbomachinery and Propulsion Systems Team. Member AIAA.
†Research Aerospace Engineer, Combustion Branch, Mail Stop 5-10.

(CARS) is an example of a popular diagnostic technique which uses a nonlinear signal generation process with the parametric amplification. Numerous efforts have been devoted to advance the science and technology of CARS for applications in thermal fluids including combustion [14–18]. Both vibrational and pure-rotational CARS methods are capable of measuring spatially and temporally resolved temperatures in practical combustion environments [19] and their capabilities have been greatly improved [20] The CARS technique has distinct advantages in spatial and spectral filtering, improved immunity to optical interferences, and can even be used in a sooty environment due to the fact that the CARS signal is a coherent, strong laserlike beam. The disadvantages of CARS are primarily its complexity and the ability to probe only one species per laser wavelength. In contrast, spontaneous (also called linear) Raman spectroscopy requires only one laser wavelength to probe multiple species (multiscalar) while being much simpler to implement than CARS. However, spontaneous Raman scattering is an inherently much weaker linear scattering process and is more prone to optical interferences. Because of the spontaneous Raman spectroscopy technique's multiscalar measurement capability, it continues to be a valuable tool for many combustion experiments as an alternative to CARS [11–13,20–24]. Although spontaneous Raman signals are inherently very weak, one can expect high-quality Raman scattering data with good signal-to-noise ratio using either ultraviolet laser excitation [23,25,26] or visible laser excitation in conjunction with a high-performance optical setup [27,28]. With such optimization, the technique can provide spatially and temporally resolved information in a single-shot manner with a sufficient level of accuracy. When single-shot data acquired by point measurements are collected over a period of time in a nonsteady or turbulent environment, the data will form so-called "scatter plots" of the multiple scalars versus mixture fraction, which are suitable for validating computational models of turbulent combustion [8,9,12,13,21]. Multidimensional cross correlations of the scalar can also be observed in the form of a correlation scatter plot. Such correlation scatter plot data can be further analyzed to obtain the probability density functions (PDFs) of the correlated scalar properties.

Spontaneous Raman scattering for combustion diagnostics also offers practical benefits. It is capable of working with only a single wavelength, a single beam, and even a single optical access port if the backscattered collection mode is used. Because spontaneous Raman scattering is a linear optical process, the measurements are typically less complicated and less expensive when compared to nonlinear optical techniques such as CARS. These facts attract a great deal of interest from researchers using it for applications related to aviation combustors [29,30]. Recently, a single-shot one-dimensional spontaneous Raman spectroscopy was successfully applied in a gas-turbine model combustor operated with natural gas fuel at elevated pressure up to 10 bar for thermochemical state analysis in the primary zone [31].

The present research uses spontaneous Raman spectroscopy to provide quantitative species and temperature data in a realistic combustor at elevated pressure for the validation of chemically reacting computational fluid dynamics codes such as the National Combustion Code being developed by an industry-government team [32]. Our approach is to perform a series of fundamental combustion experiments with increasing chemical complexity, which eventually reflect aviation jet fuel, using a state-of-the-art high-pressure turbulent combustion facility. As the first step of this research, a realistic swirl-stabilized fuel-lean methane-air flame is investigated at moderate pressure. Methane-air combustion produces chemically simple first-case for combustion code validation compared to more realistic kerosene-based jet fuels.

II. Experimental Description

A. High-Pressure Swirl-Stabilized Gaseous Flames

The experiment was conducted in a high-pressure optically accessible combustion test facility fitted with a swirl-stabilized nonpremixed methane-air combustor operating at a pressure of 5.0 atm. The flame was operated at a global equivalence ratio, $\phi = 0.56$, which approximately corresponds to the steady flammability limit of a freely propagating methane-air flame at a moderate strain rate (a few hundreds of s^{-1}) [33]. The burner generates highly strained turbulent gaseous flames based on the NASA-developed lean-direct-injection (LDI) configuration [34]. The schematic diagram of the single-element LDI burner nozzle is shown in Fig. 1. The burner nozzle consists of a 60-deg counterclockwise swirl vane element (swirl number 1.27) for combustion air and integrated into the existing high-pressure burner facility hardware [35,36]. The burner nozzle has a fuel injector that comprises six radially aligned plain jets (1.14 mm diam) angled at 45 deg to the burner axis, but perpendicular to the local flow path of air passing by. Several groups have adopted the LDI configuration for studying realistic turbulent gaseous [37] and spray combustion [38,39]. To minimize unnecessary complications regarding code validation, a single-element LDI was used in the present work instead of the multiple-injector configuration. This particular LDI burner typifies that used in the primary zone of advanced low-emissions gas-turbine combustors. We expect that intensive experiments on this platform will provide the most valuable validation data in a realistic turbulent combustion at simulated engine conditions particularly with regard to the scalar formations over a range of inlet air temperature, fuel mixture, or swirl strengths in the future.

The LDI burner was mounted inside a high-temperature air-cooled liner casing within the high-pressure combustion rig. The oxidizer air and the CH_4 fuel were provided by compressed gas cylinder arrays. The flow rates of the oxidizer air and fuel were precisely controlled within $\pm 1\%$ accuracy using a valve-switched array of three critical-flow venturis, fitted with pressure transducers and computer operated precision pressure regulators and valves to provide both high accuracy and a high dynamic range for the gas flows. The sonic flow venturis also serve to limit the maximum flow of the fuel in case of a downstream drop in rig pressure (as in the case of a burst disk rupture event). The averaged flow rates of the oxidizer air and the fuel during the experiment were 1040, and 61.0 standard liters per minute. The oxidizer air was "preheated" at approximately 430 K before the swirl vane due to heat conduction from the burner element while the facility was not equipped with an air preheater at the time of experiment. A retractable, high-energy surface-discharge aircraft style igniter system is used to ignite the burner.

Ambient-temperature cooling air was introduced at the bottom of the rig for liner cooling and also at the upper side as a "quenching"

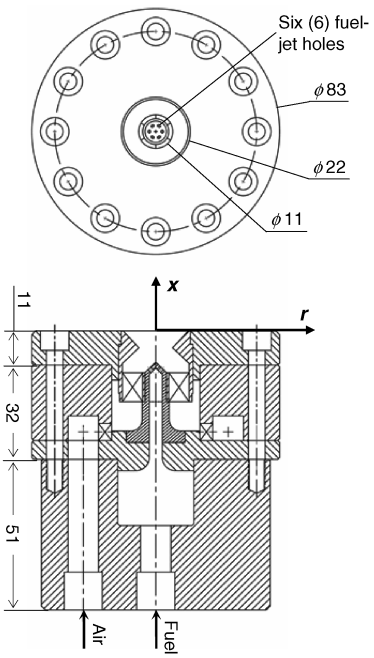

Fig. 1 Schematic drawings of LDI burner nozzle: top and side view (cross-section diagram). Units are in mm. The axial and radial directions are indicated by *x* and *r*, respectively.

flow to directly cool the hot exhaust gases. The pressure of the burner rig was maintained via a high-temperature backpressure valve mounted at the top of the chamber, which is remotely operated by a stand-alone closed-loop process controller. The rig pressure was kept at 5.0 atm in the present work although the burner rig is designed for up to 60 atm. The pressure was stabilized within $\pm 1\%$ accuracy for each condition. For optical access, the burner rig has four 44-mm-thick ultraviolet grade fused silica windows with a clear aperture of 75 mm. Further details on the combustion systems are described elsewhere [35,36].

The measurements were made at several locations downstream from the burner exit, radially from $r = 0$ to 14 mm and axially from $x = 9$ to 33 mm. These measurement locations were chosen to provide a reasonable amount of coverage of the primary flame zone and to also reach sufficiently downstream to a zone that represents the fully reacted postflame region.

B. Single-Shot Spectrum Measurement of Raman Scattering

Another challenge with spontaneous Raman spectroscopy in elevated pressure systems is the requirement of windows and pressure vessel walls in the vicinity of the collection optics. In addition to limiting optical accessibility through the clear apertures of the windows, such environments inherently have much higher levels of elastically scattered stray light that leaks into the diagnostic system due to light reflections at windows, combustor walls, or Mie scattering from dust particles. The elastically scattered stray light in practice is almost impossible to completely eliminate, thus the use of molecular Rayleigh scattering as a temperature diagnostic of very limited utility. This prompts us to rely on Raman-based spectroscopic thermometry using N_2 Stokes/anti-Stokes ratio and/or frequency-domain Raman thermometry techniques [40].

Although the high-pressure environment gives us an advantage in gaining a stronger Raman signal due to higher molecular number density, there were concerns regarding pressure broadening for line shapes of the Raman spectra. However, our theoretical simulation of the molecular collisional broadening effect of the major species [41] and combined with data measured at 30 atm [36] showed that the pressure effects were negligible compared to the typical instrumental broadening function of a relatively low-spectral resolution Raman spectrograph used in a multiscalar combustion diagnostic application. Measuring an overall spectrum provides an opportunity to confirm the spectral shape and a validity of pixel integration for each species at a given pressure.

Regarding the excitation wavelength, several reports have addressed the utility of a few different wavelengths including Nd:YAG harmonics (II-532, III-355, IV-266 nm) [42] or KrF excimer (e.g., 248 nm) [43] in harsh environments such as hydrocarbon-rich flames or droplet-laden flames [44]. Single-shot Raman spectrum measurements have been successfully demonstrated with an image-intensified charge-coupled device (CCD) at an ultraviolet (UV) wavelength [6] in opposed-jet methane flames. In contrast, a visible Raman system remains attractive to gaseous turbulent flame studies as well as sooting flames [38] when it employs a high-power ($\sim$1 J/pulse), stretched-pulse laser excitation with a high-speed mechanical gating shutter and a high-dynamic-range CCD camera [27,40]. However, it remains challenging to achieve an acceptable signal-to-noise ratio on a single-shot basis, particularly with limited clear aperture to work with a high-pressure rig. Our first attempt of single-shot visible Raman spectrum measurements was thus made in the laboratory-scale burner with a combustor model injector.

C. Diagnostics Apparatus

Figure 2 shows a setup of our laser Raman spectroscopy apparatus. We use an injection-seeded, Q-switched Nd:YAG laser (second harmonic) for spontaneous Raman scattering excitation. The laser provided approximately 500-mJ, 532-nm pulses (8.4 ns full width half maximum, or FWHM) at a 10-Hz repetition rate. Using multiple ring cavities, the laser pulses were then temporally "stretched" to about 75 ns (FWHM) with approximately 10% of the peak power of the input pulse, while retaining 83% energy throughput efficiency

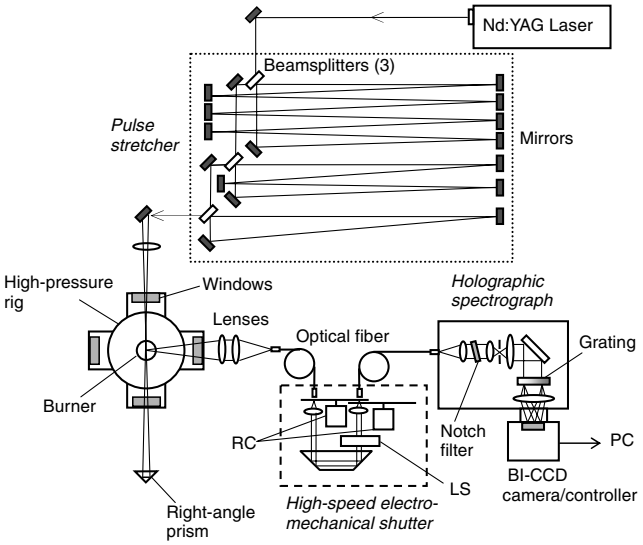

Fig. 2 Schematic of high-performance Raman scattering apparatus. There are four main components to the system: frequency-doubled Nd:YAG pulsed laser, pulse stretcher, high-speed electromechanical shutter, and spectrograph/backside-illuminated CCD camera. Legend—RC: rotary chopper motor/blade combination; LS: leaf shutter; PC: personal computer.

[28]. The reduced peak power prevented laser-induced spark/plasma formation at the probe volume. A 750-mm focal lens focused the output of the pulse stretcher to the probe volume waist diameter of approximately 1 mm. To effectively double the probe volume energy, the laser beam was backpropagated through the probe volume at a small crossing angle using a 400-mm collimating lens and a right-angle prism.

The vertically polarized Raman scattering signal from the probe volume was collected at a 90-deg angle relative to the beam-propagation direction using a standard 35-mm format camera lens (85 mm $f/1.4$). Note that the maximum solid angle of the current collection optics is actually only $f/3.9$. This is a consequence of the 295-mm window standoff distance, and 75-mm effective diameter. The collected light was then focused onto a silica optical fiber (0.4-mm core diameter, 0.22 NA). An electromechanical high-speed shutter [45] synchronized to the 10-Hz laser pulses was used to gate the light emerging from the fiber. The shutter system in this study provided a 24-μs gate time (FWHM) with 0.4 μs jitter through a 12×0.8 mm^2 clear aperture with an overall 55% optical throughput including fiber transmission losses. The high-speed shutter system reduced the effects of background light interferences by a factor of about 1000 compared to a conventional electromechanical leaf shutter. The optically gated light from the shutter was directed to the Raman spectrograph using a custom-made fiber bundle consisting of seven 0.1-mm core (0.22 NA) silica optical fibers arranged in a circular pattern to match the 0.4-mm-diam core of the input fiber into the shutter. The output of the fiber bundle was arranged in a 7×1 linear array and aligned to match the 0.1-mm-wide input slit of the spectrograph. The Raman signal was dispersed with an axially transmissive visible-wavelength spectrograph ($f/1.8$ maximum aperture, 85-mm focal length) fitted with a holographic notch filter to attenuate the Rayleigh scattering component of the signal. A volume phase holographic transmission grating with a 15.9 nm/mm reciprocal dispersion at the detector plane dispersed the signal into a spectrum which was detected by a nonintensified, liquid-nitrogen cooled (-120°C), backilluminated CCD camera (1340×100 array, 20×20 μm^2 pixels). The effective probe volume was approximately cylindrical in shape with approximate dimensions of 0.5 mm diam $\times$ 1.6 mm long. The spectrograph we used was designed to capture a Raman spectrum with a relatively low resolution (1.3 nm or 35 cm^{-1}) using a 0.1 mm slit over a wide spectral range (400–750 nm). This specification was best suited for a multiscalar measurement as it can conveniently measure the

vibrational Stokes and anti-Stokes bands of the major combustion products as well as the rotational envelope component of N_2/O_2.

The backilluminated CCD camera and electromechanical shutter combination were selected over an intensified CCD camera because it provides greater than 90% detector quantum efficiency (QE) with a 200,000 photoelectron dynamic range that was digitized at 16 bits of resolution. The simultaneous requirements of high QE and high dynamic range were critical for accurately capturing the full range of weak (vibrational) and strong (pure-rotational) Raman signals and its background interferences as they appear in high-pressure flames. Each single-shot data were binned on chip over 50 vertical pixels to increase signal-to-noise ratio. Schematics of the Raman diagnostic system and its performance have also been described in detail previously [35,36].

D. Multiscalar Signal Reduction

The spectrally resolved raw Raman spectra measured using the above single-shot apparatus were first digitally filtered shot by shot using a Gaussian low-pass filter algorithm to remove random detector noise. The spectra were then processed by applying a conventional spectral response calibration curve from a National Institute of Standards and Technology traceable calibration lamp; the Raman signals in the spectra were integrated over a certain range of CCD pixel region (or wavelengths) that captures the main vibrational peak of each major species, or the so-called superpixel formalism. From this superpixel integration, the Raman scattering intensities in the radiance unit for the four major species, that is, N_2, O_2, CO_2, and CH_4, were determined. The Raman signals were then converted into the molecular number density (molecules/cm^3) [hereafter denoted $n(i)$], where i is the species) using the inverse calibration matrix formalism described elsewhere [22]. The baseline for the superpixels was defined shot by shot in the Raman-free region of the background signal. Several factors including the inherently weak signal level in the single-shot measurements, the fuel-lean operation, the limited apertures of the optical access, and relatively higher level of background flame luminescence at the red side (>640 nm) did not allow reliable data of the other major species such as CO (601 nm), H_2O (661 nm), or H_2 (683 nm). Because of this fact and incomplete calibration experiments at the time of testing, we adopted a simpler formation of the calibration matrix using a linear nontemperature dependent overlap (cross talk) rate [25] with calibration factors based on cold gas flows. The CO_2 spectral overlap onto O_2, which was considered critical to our present analysis, was corrected in this process. Spectral overlaps of these undetected species have a minor impact on N_2, O_2, or CH_4 due to the fact that the burner was operated at close to the lean limit of methane-air combustion. We acknowledge that the simplified calibration matrix imposed additional systematic uncertainty in our current data reduction process. However, the uncertainty associated with the simplified calibration was not estimated in this study. Other sources of errors include the quality of the cross-talk calibration matrix, the potential drift of the probe volume over time during the measurements, or the uncertainties due to incomplete optical background compensation. According to our shot noise analysis of the single-shot signals, standard deviations of the vibrational Raman signals of N_2, O_2, and CH_4 are 4.6, 11.7, and 7.8%, respectively [40]. Occasionally the background from intense spark emission due to a laser-induced breakdown overwhelmed the Raman signals and thus disqualified some single-shot events (typically 2.5% of the total number of shots) from any further reduction process.

Thermodynamic temperatures T and K were determined through a rotational Raman bandwidth method [40] by taking advantage of the intense rotational bands. This thermometry approach is based on the pure-rotational Raman scattering of N_2 collected at low-spectral resolution which is complementary to the vibrational Raman thermometry methods typically used for multispecies detection with the vibrational bands. With the aid of spectroscopic simulations of Raman spectra, the thermometry technique used in the present work was realized by measuring the envelope or effective rotational bandwidth of the pure-rotational spectrum observed at lower spectral resolution (on the order of 10^0 nm or 10^1 cm^{-1}). Influences from the pure-rotational O_2 scattering onto the N_2 were compensated by accurate spectral simulation, and its effect on the temperature determination process was implemented using a species-weighted interpolation method. The standard deviation of the single-shot temperature measurements in the current experiment was found to be 7.7%.

III. Results and Discussions

A. Single-Shot Multiscalar Data

Typical single-shot Raman spectra acquired in the methane LDI flame at a 10-Hz repetition rate are shown in Fig. 3. The relatively stronger pure-rotational spectra observed across the excitation wavelength (centered at 532 nm) represent the anti-Stokes and Stokes bands of the N_2/O_2 mixture with a potentially minor influence from underlying pure-rotational CO_2 bands [40]. The vibrational O_2 spectra are observed at 580 nm while it overlaps with the vibrational CO_2 spectra around 574 nm. The vibrational N_2 Q-branches at 607 nm are observed rather steadily while the vibrational CH_4 spectra around 630 nm have a large shot-to-shot variation in their intensity. There is no unique or persistent background observed such as C_2 LIF and that is generally true throughout the measurement locations. The shot-to-shot variations in the Raman signal for each species (O_2, N_2, and CH_4), which clearly exceed the measurement uncertainty, indicate an unsteadiness of the flame.

The effectiveness of the multiscalar measurements for statistical analysis is illustrated in the three-dimensional (3-D) scatter diagrams (or scatter plots) of Fig. 4, which shows the three key scalars, that is, T, O_2, and CH_4, deduced from the single-shot signals measured at two locations. The 3-D scatter plots display the direct correlations among the scalars, showing a clear difference in the level of turbulence-derived fluctuations. As shown in Fig. 4a, the data points measured at $(r, x) = (14\text{ mm}, 9\text{ mm})$, a location where a strong shear flow may exist due to a combination of the direct fuel injection and swirl flow, present a wide scatter over the three scalar dimensions, suggesting a turbulent state. Most of the data points measured at the highest location on the burner axis, that is, $(r, x) = (0\text{ mm}, 33\text{ mm})$, however, show little scatter as shown in Fig. 4b, which indicates a thermochemically homogeneous state. The difference between the two distinct thermochemical states can be specifically recognized in the PDF diagrams of the O_2 and CH_4 as shown in Fig. 5 along with the correlation scatter plot. The PDFs were constructed from the supplied histogram data using a nonparametric kernel-smoothing method. Thus the PDF shown in

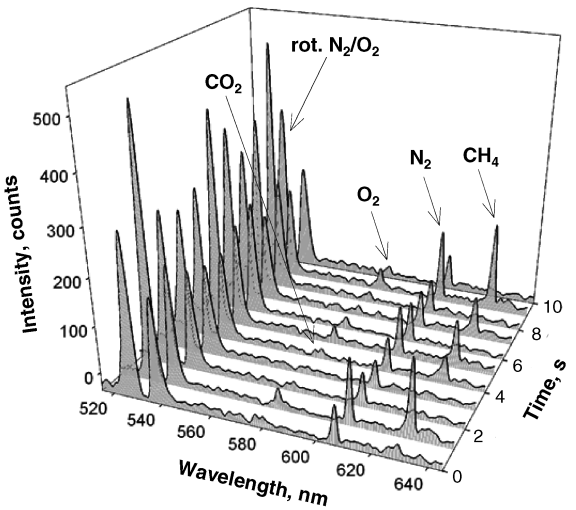

Fig. 3 Typical single-shot Raman spectra (532 nm excitation) measured in the turbulent methane–air flame. Eleven shots are shown out of a total 400 shots obtained by the measurement at $(r, x) = (10, 9)$.

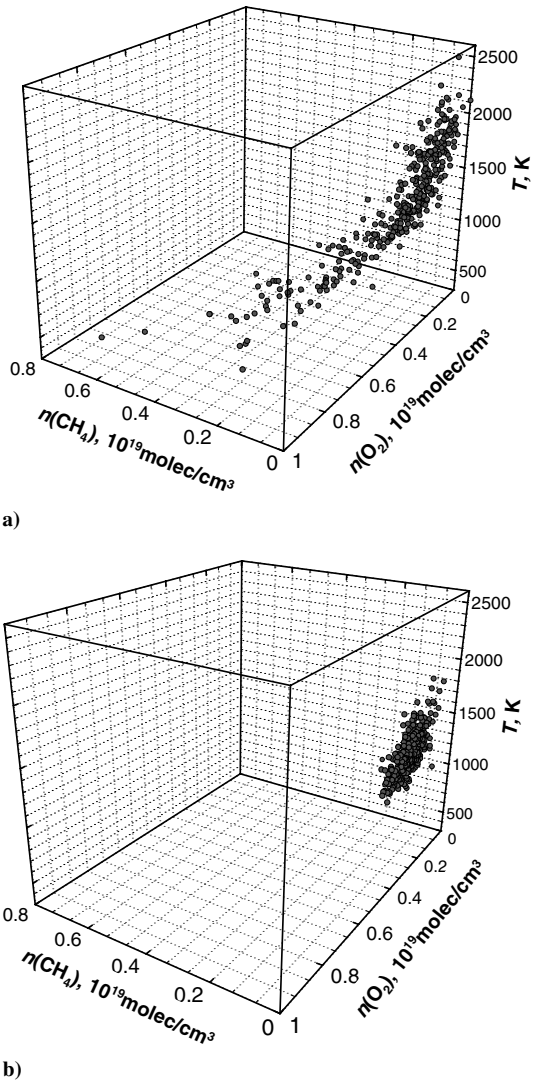

Fig. 4 Multiscalar (fuel–oxidizer–temperature) scatter plots, analyzed from the single-shot data (400 shots) measured in the turbulent flame. a) Measurements at $(r, x) = (14, 9)$; b) measurements at $(r, x) = (0, 33)$.

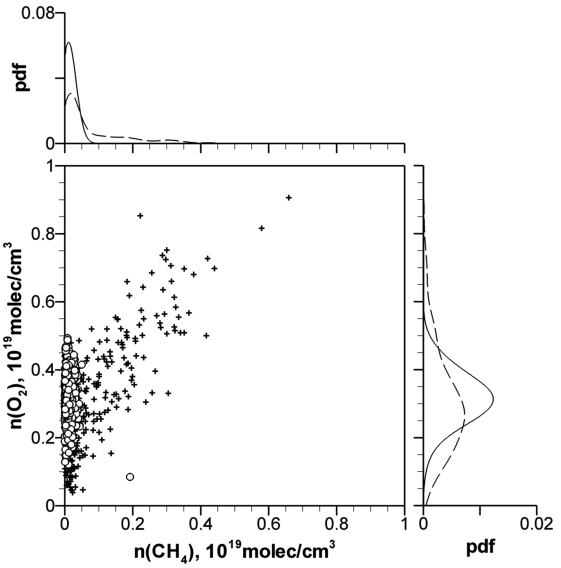

Fig. 5 Scatter plots of O_2–CH_4 correlations, observed in the turbulent flame and the probability density function of CH_4 (top) and O_2 (right). Plus symbol and dashed line: measurements at $(r, x) = (14, 9)$; white circle and solid line: measurements at $(r, x) = (0, 33)$.

this paper is considered as a generalization of the histogram. The minimum scatter observed at $(r, x) = (0\text{ mm}, 33\text{ mm})$ in the $n(CH_4)$ over a mild variation of the $n(O_2)$ results in the narrow PDF distribution of the $n(CH_4)$ centered at the vicinity of zero value while that at $(r, x) = (14\text{ mm}, 9\text{ mm})$ spreads widely toward the higher concentration.

B. Multiscalar PDFs and Correlations

From the measurements at multiple locations, one can track the scalars as a function of position using their PDFs. Figure 6 shows a trend of the PDFs of the three scalars on the burner center axis with their averaged value. It is known from the figure that almost all of the PDFs of the O_2 and the temperature in these locations have a normal distribution, particularly at higher points where a much more homogeneous postcombustion zone can be expected to be located. For these two scalars, the mean values correspond well to the most probable value of the PDFs, that is, the peak location of the Gaussian-like profiles. The CH_4 PDFs, in contrast, have "truncated" distributions with peaks that are located close to zero (an exponential-like profile), showing the higher probability of low concentrations. The mean values of the $n(CH_4)$, which are slightly off from the most probable values (peak), gradually decrease as the measurement height increases. This is naturally understood by the fact that the flame was running at fuel-lean conditions; thus the fuel CH_4 tends to be almost fully consumed as it approaches the postflame zone region.

We further extend our thermochemical analysis by observing the spatially mapped multiscalar diagrams including the temperature histograms accompanied with the PDFs of CH_4, and O_2, and 3-D scatter plots of the triple-scalar correlations (hereafter denoted as "scalar triplets") shown in Figs. 7–10. From these multiscalar diagrams, critical insight into the characteristics of the fuel–air mixing in the current LDI burner can be observed. Figures 7–9 show the variations of the PDFs and the scatter plots along the radial direction at the three different heights, and Fig. 10 shows the axial direction on the burner center axis. The PDF (and the histograms) of temperature measured in a region closest to the burner face ($x = 9$ mm), in a region of the burner with relatively poor mixing, shows the largest variation in temperature ranging from the room temperature (~300 K) to almost the adiabatic temperature of the 5-atm CH_4-air flame at $\phi = 1.0$ (~2300 K) as seen in Fig. 7 (left column). This temperature variation is more obvious toward the outer locations of the burner ($r = 8$–14 mm). The reason for such large temperature variations is illustrated in the scalar triplets of Fig. 7 (right column). Notice that the data have two groupings. The first group consists of lower-temperature data points with higher fuel (CH_4) and oxidizer (O_2) concentrations, which indicate unburned fuel–air mixture. The existence of the cold, unburnt pockets suggests the possibility of a certain degree of incomplete combustion around the edge of this flame. The second group can be attributed as resulting from the dense region of data points with higher temperature (>2100 K) located at lower fuel and oxygen concentrations. This grouping of data given in several locations indicates combustion processes that took place near stoichiometric fuel–air ratio contours, the so-called "hot spots." As seen in Fig. 7 (middle column), the large variation in the number density of the species in these outer locations results in the wider O_2 PDF profile as well as the long-tailed CH_4 PDF profile. We believe that these large variations in the three key scalars are evidence of swirl-enhanced turbulent fluctuations in fuel–air mixing and its subsequent reaction. Another notable feature is the bimodal shape of the temperature PDF found at the radial locations $r = 4$ mm through $r = 12$ mm in Fig. 7. Such bimodal temperature PDFs represent oscillatory behavior between two states (i.e., the lower or higher temperature zones) and thus imply a certain level of combustion instability, possibly due to the precessing vortex core [46]. It is noted that we obtained a few data points with unrealistic temperature which exceeded the highest adiabatic flame temperature in stoichiometric methane–air combustion. This is most likely due to

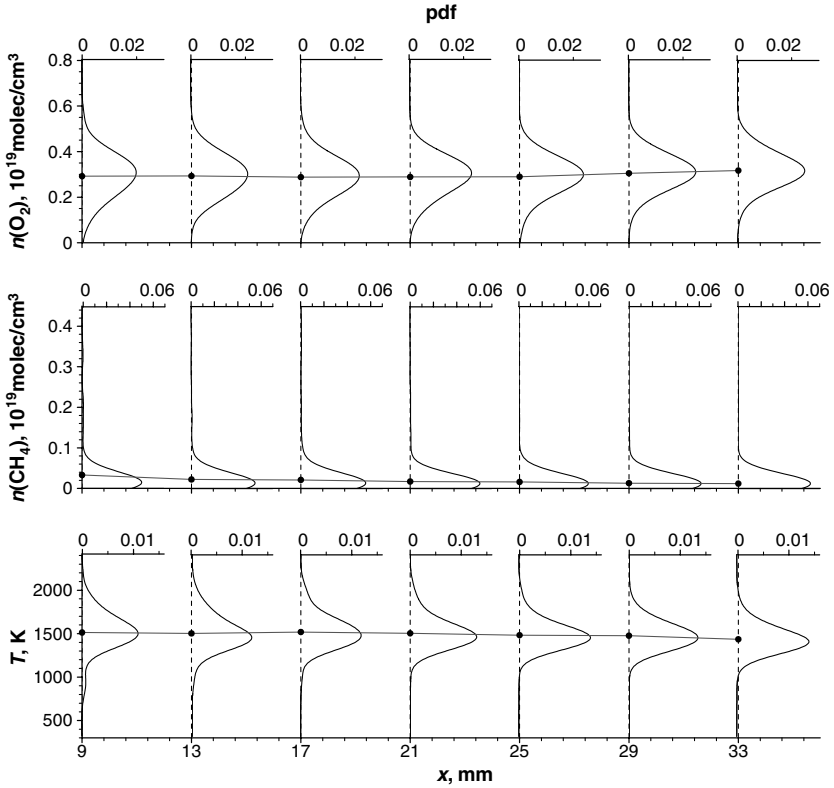

Fig. 6 PDFs of temperature, CH_4, and O_2 at selected axial locations (from $x = 9$ mm to $x = 33$ mm) along the burner centerline ($r = 0$). Averaged values are plotted by black circles.

the measurement uncertainty of the present thermometry described above.

As observable from the scalar triplets shown in Fig. 8 ($x = 13$ mm) and Fig. 9 ($x = 17$ mm), the higher the axial location, the less scatter there is. This can be explained by the fact that the primary turbulent mixing zone progressively becomes more well mixed farther downstream of the burner face. Correspondingly, at the higher location $x = 17$ mm, the temperature PDFs become less bimodal, and the CH_4 PDFs show narrower distributions with very short tails. These mild variations indicate that the LDI flame approaches a homogeneous state around the height $x \sim 17$ mm. This perspective is supported by the axial transition of the thermochemical state shown in the multiscalar analysis along the burner axis in Fig. 10, where the center recirculation zone is likely to be formed by a vortex breakdown process [47,48] with steady heat release. Figure 10 also shows scalar triplets that have a bimodal temperature PDF near the burner surface ($x = 9$ mm), while scalar triplets with less scatter and narrower PDF distributions of temperature were measured farther downstream. In particular, at the highest location ($x = 33$ mm), the scatter in the scalar triplets is substantially reduced as this postflame zone exhibits what appears to be a steady fully reacted region, which is evident in the highest probability of the $n(CH_4)$ being almost zero (that is, almost no fuel residual) with the narrowest, normal (Gaussian-like) PDF distribution of temperature. The scatter of the $n(O_2)$, which is realized from its relatively unchanged, wider PDF distribution, in this postflame zone can be explained by the fact that the flame is fuel lean, and there may be a small influence from air entrainment into this region from the cooler, outer regions of the flame.

To grasp an understanding for the overall feature of the mixing, the single-shot scalar data obtained over all of the current 28 measurement locations, which totaled approximately 11,000 samples, are summarized in the $n(CH_4) - n(O_2)$ correlation of Fig. 11 and the $T - n(CH_4)$ correlation of Fig. 12. Coexistence of the CH_4 and the O_2 in Fig. 11 is a compelling evidence of a fuel–air premixing state and has a consequence that the current flame regime can be classified as partially premixed [13]. Overall, the trend of the premixed fuel–air mixture follows the criteria of $\phi = 0.56$, meeting the designed global equivalence ratio. This indicates that the flame demonstrated a high degree of turbulent premixing that occurred within a short distance from the injector tip.

According to Fig. 12, approximately 80% of the data, represented by a dense cluster, exhibits very low methane concentrations (less than 0.05×10^{19} molecule/cm^3), while the temperature is between 1200 and 2150 K. Thus, the majority of the data is considered as a complete reaction or near-complete reaction as they demonstrate almost no fuel residual with temperature much higher than the ignition point of the gaseous methane. It is assumed that this primary reaction zone ($x < \sim 3R$, where R is the inner swirler diameter) created by the LDI configuration contributes to the stabilization of the flame. However, in this group of near-complete combustion, there are a significant number of data points that exhibit temperatures lower than the adiabatic temperature ($\sim$1590 K) of a 5-atm lean-limit CH_4 air. This can be explained from the fact that a highly stretched flame with the strain rate of a few hundreds s^{-1}, which is not an unrealistic assumption for the current swirl-stabilized flame, should have a maximum temperature reduction on the order of several hundred Kelvins [49,50]. Another possible explanation is the presence of heat loss to the burner surface [35].

In Fig. 12, there are also a considerable but not significant number of data points displaying residual fuel, with intermediate temperatures between the ignition point ($\sim$810) and $\sim$1300 K. According to Figs. 7–10, data points with intermediate temperatures tend to be observed in the shear layer presumably formed along the orientations of swirl flow and fuel injection. In a previous report on swirl-stabilized natural gas combustion [13], such features have been addressed as evidence of partially reacted mixtures. These partially reacted zones have been explained from possible events of local flame extinction and/or ignition delay, resulting from effects of turbulence–chemistry interaction. We agree with this viewpoint that local flame extinction in nonpremixed flames can lead to a significant reduction in mixture gas temperature from adiabatic equilibrium [9,13]. Also, as shown here, the fuel–air mixture has a large variation in gas composition and temperature and is subject to ignition delay.

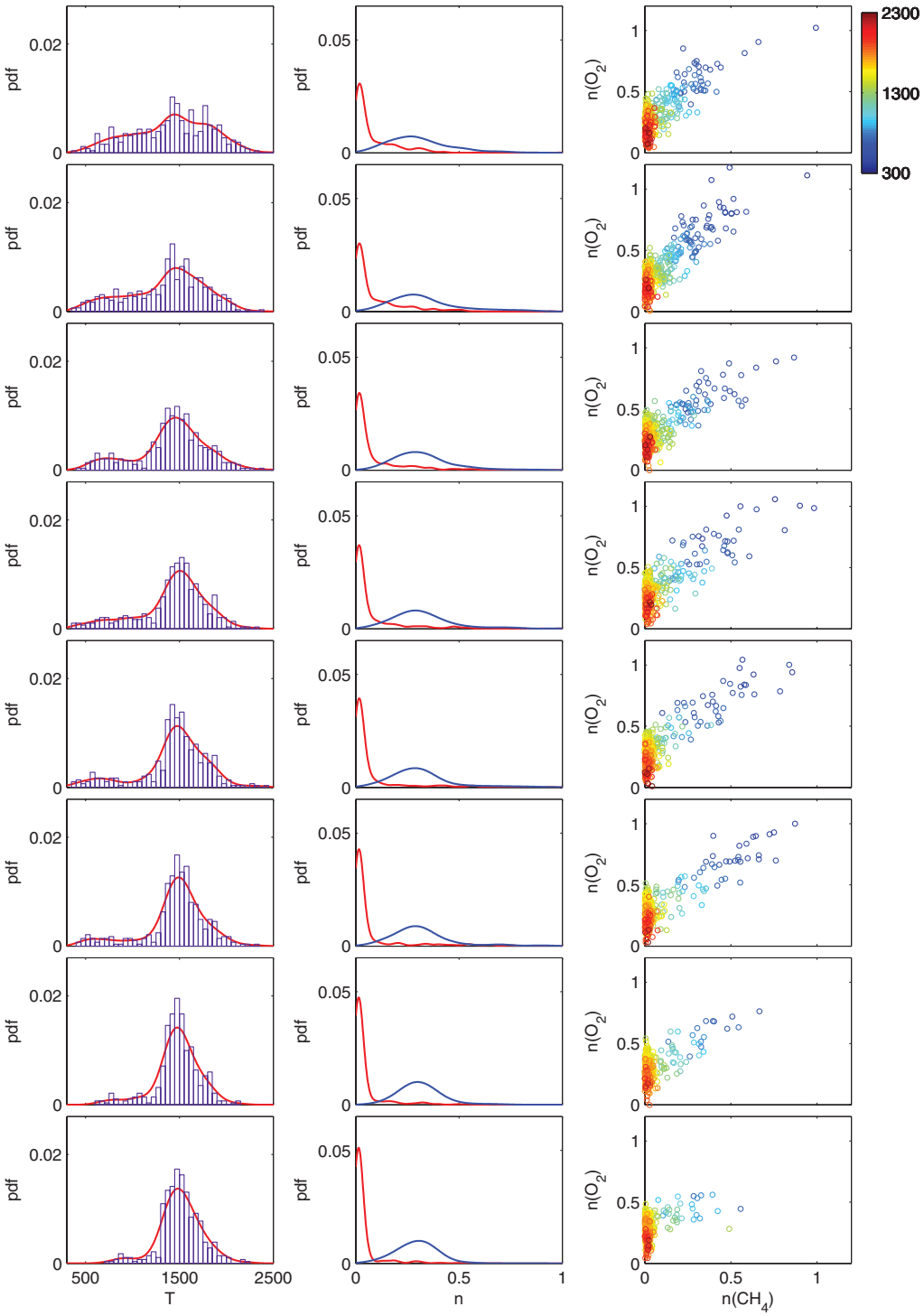

Fig. 7 Thermochemical multiscalar analysis at different radial locations from $r = 0$ (bottom row) to $r = 14$ (top row) with the increment of 2 mm at $x = 9$. Left column: histogram and PDF of temperature. Middle column: PDFs of species number density (red: CH_4; blue: O_2). Right column: triple-scalar correlation, with temperature in color scale.

Ignition delay strongly depends on the initial temperature of the mixture and the chemical kinetics [51]. The ignition delay time for atmospheric fuel-lean CH_4/air mixtures at temperatures below 1300 K has been estimated on the order of 10^0–10^1 ms according to a finite-rate chemistry flame simulation [13]. Compared to this estimated ignition delay, the characteristic time scale of the flowfield [52] in our LDI burner is an order of magnitude smaller, approximately 0.2 ms. This time scale was estimated by a calculation based on a typical flow velocity ($\sim$45 m/s) derived from the mean airflow rate and the burner height ($\sim$10 mm). Thus, ignition delay can have a substantial influence on flame propagation in the current burner configuration. It should be noted that ignition delay may become less significant at higher pressures because ignition delay has inverse dependency on ambient pressure [50].

Figure 12 shows that less than 3% of the data are found to be below the ignition-point temperature with higher $n(CH_4)$, which is classified as a "cold" fuel–air mixture. This is known from the observed bimodal temperature PDFs as seen in Figs. 7–10. This small amount of unburned mixture exists mainly in the locations where a recirculation flow is likely to occur. Therefore, the gas mixture could possibly be redirected into the active reaction zone by the recirculation flow and subsequently be consumed. The existence

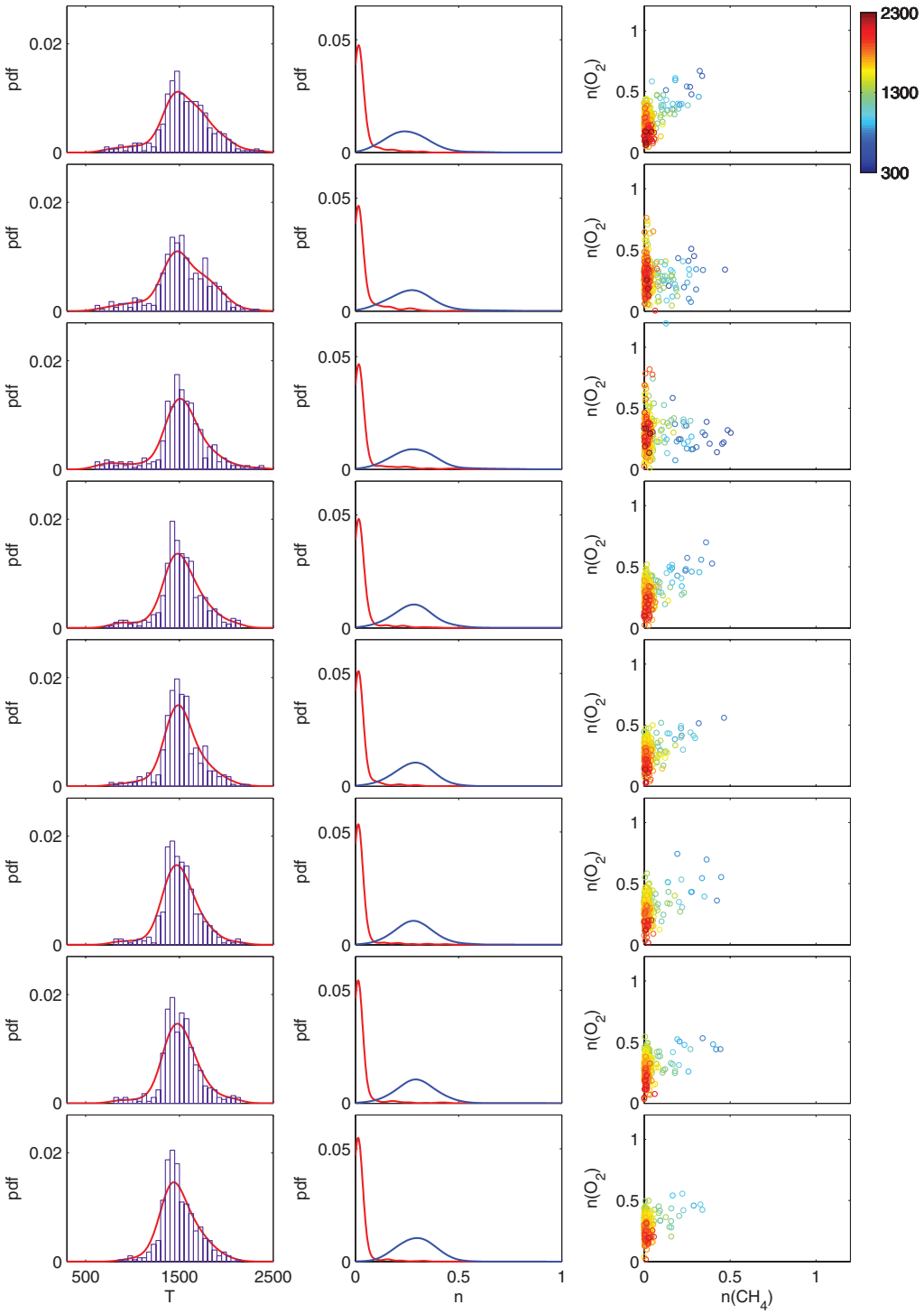

Fig. 8 Thermochemical multiscalar analysis at different radial locations from $r = 0$ (bottom row) to $r = 14$ (top row) with the increment of 2 mm at $x = 13$. For more details, refer to the caption of Fig. 7.

of stoichiometric fuel–air mixture pockets and its subsequent reaction at close to the adiabatic temperature (2257 K) is also evident from the data presented in the preceding figures.

IV. Conclusions

In light of the high demand for high-quality data from code-validation experiments in a realistic gas-turbine combustor, we provide an initial attempt to provide quantitative multiscalar information in a swirl-stabilized nonpremixed combustion system at elevated pressure. A single-element LDI-type research burner was used as a first test for a simplified yet critical validation case using gaseous CH_4 fuel at a moderate pressure of 5 atm. For this objective, single-shot pointwise spontaneous Raman spectroscopy using a visible pulsed laser and multichannel array detector was employed. Thermodynamic temperatures in the flame were determined by using the newly developed pure-rotational Raman thermometry using the effective N_2/O_2 bandwidth measurements. In addition to the temperature data, species concentrations (molecular number density) of the fuel (CH_4) and the oxidizer (O_2) were acquired. The uncertainty of these measurements ranges between 7 and 11%, which is an acceptable level from the standpoint of code-validation studies.

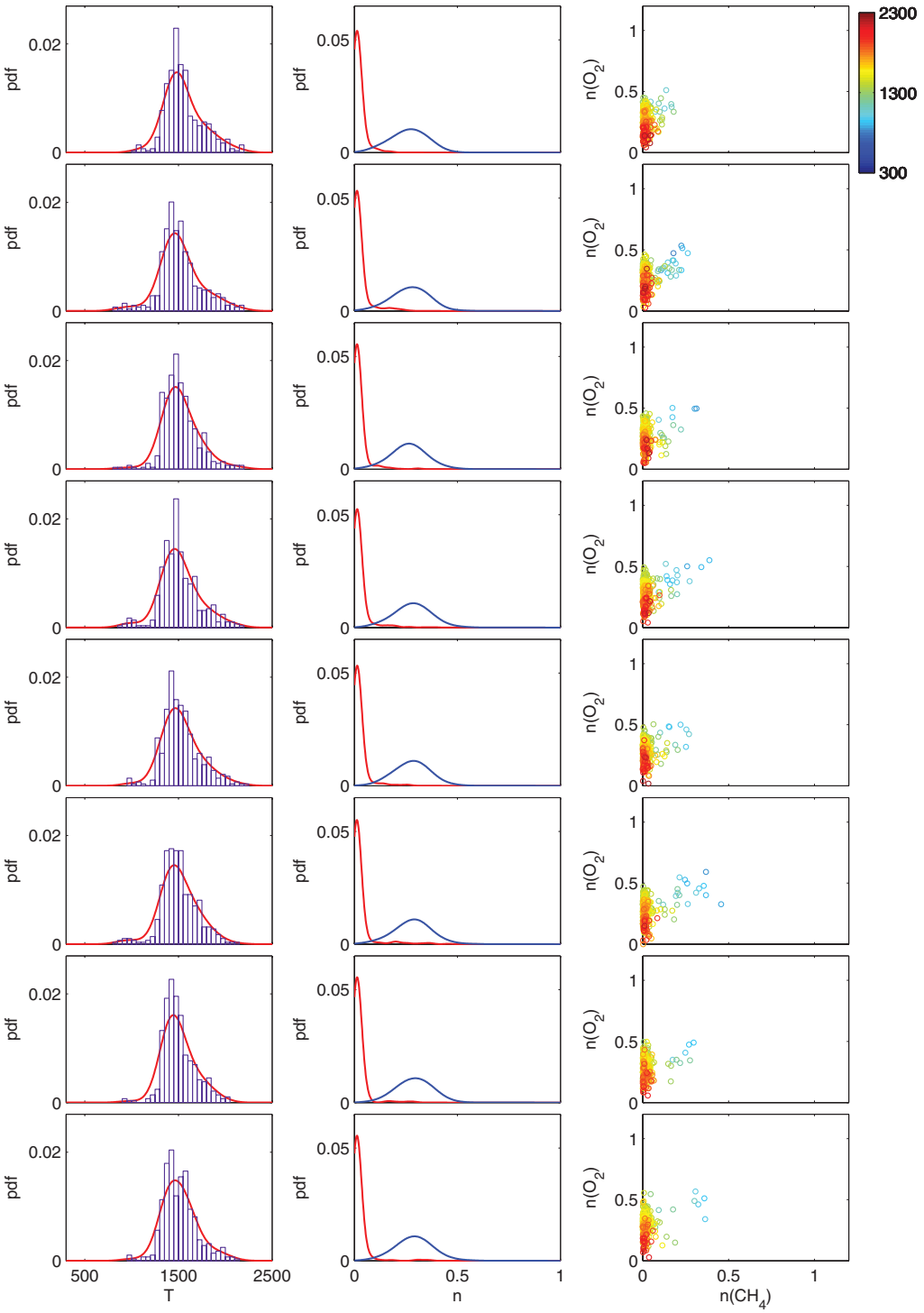

Fig. 9 Thermochemical multiscalar analysis at different radial locations from $r = 0$ (bottom row) to $r = 14$ (top row) with the increment of 2 mm at $x = 17$. For more details, refer to the caption of Fig. 7.

The time-resolved multiscalar data measured across the primary reaction zone of the combustor allowed us to analyze spatially mapped probability distributions. These probability distributions are best described by the PDFs of the key scalar observables. Furthermore, the three-component scalar triplets, T, $n(CH_4)$, and $n(O_2)$, provided unique correlations when presented in a scatter plot format that revealed distinctly different regimes of turbulence–chemistry interactions in the flame. Profound unsteadiness in the combustion process generated by the LDI configuration was evident from the large temperature variations ranging from almost ambient temperature to the adiabatic flame temperature. A recirculation zone in the flame was identified from the associated widespread temperature PDFs which feature a bimodal shape in the outer lower locations of the burner ($r = 8$–4 mm, $x = 9$–13 mm). At the highest location ($x = 33$ mm) measured, we confirmed that the flame reached a steady fully reacted state, which was evident from the minimum scatter of the scalar triplets and the highest probability of low CH_4 concentration with the narrowest, normal PDF distribution of temperature.

The extent of the turbulence–chemistry interactions has been also addressed. The swirl-stabilized flame showed high levels of partial premixing due to the high degree of turbulent mixing achieved by the LDI configuration. As a result of the dominant partially premixed combustion regime, a majority of the measured samples indicated a

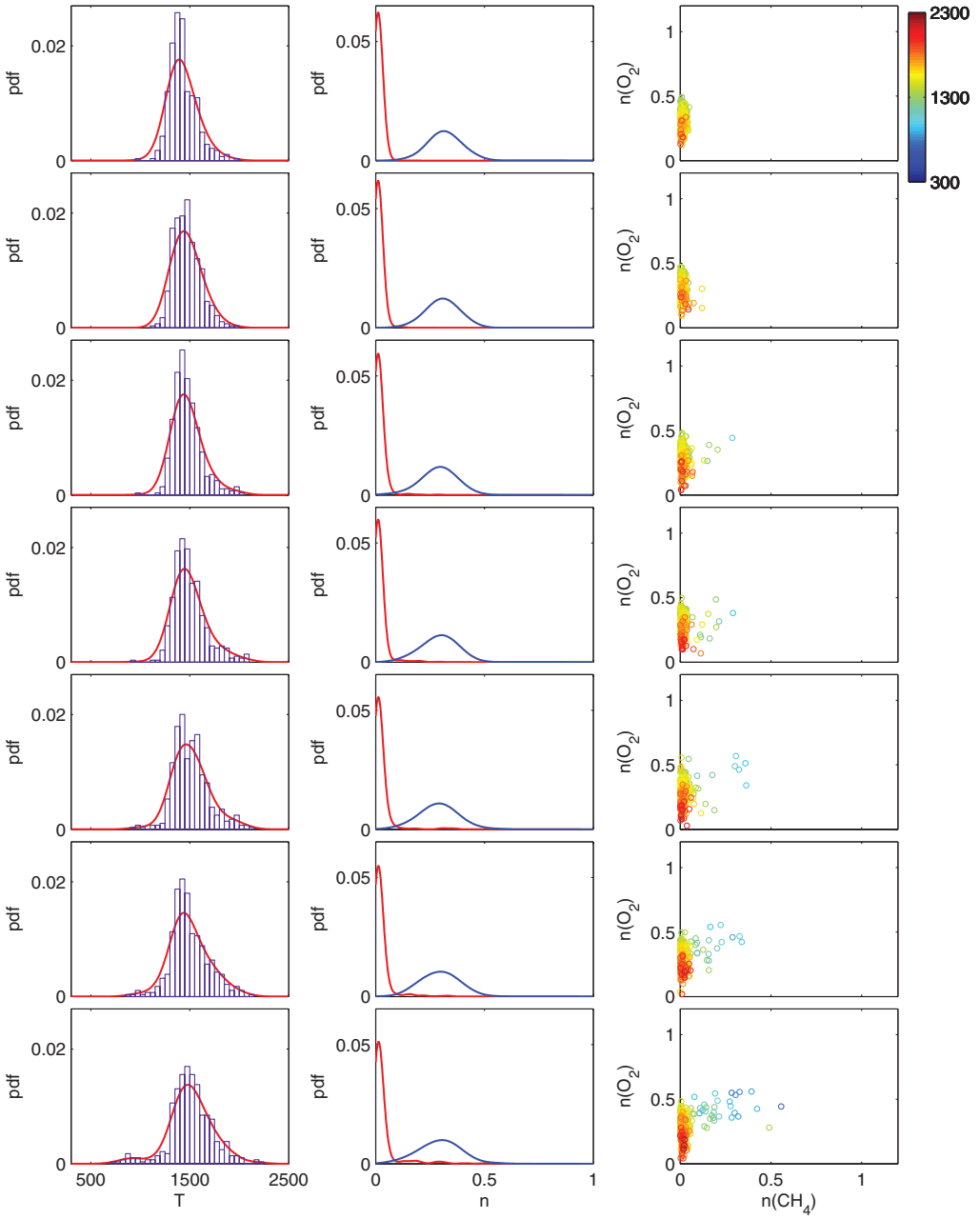

Fig. 10 Thermochemical multiscalar analysis at different axial locations from $x = 9$ (bottom row) to 33 (top row) with the increment of 4 mm along the centerline of the burner ($r = 0$). For more details, refer to the caption of Fig. 7.

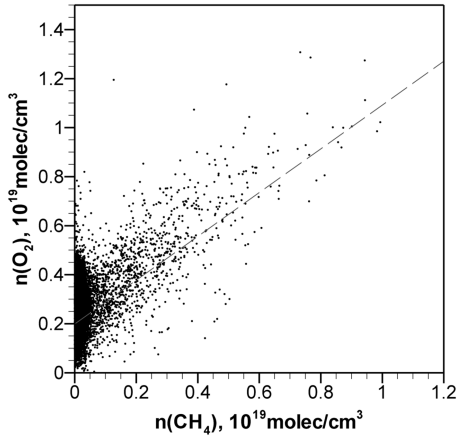

Fig. 11 Overall correlation between CH_4 and O_2 number density. The dashed line indicates the criteria which meets the equivalence ratio of 0.56.

complete or near-complete reaction, which is in favor of the design concept of the burner. The observed mixing-only conditions (i.e., preheated to below-ignition-point temperature) were observed to follow the global equivalence ratio of the flame and are further evidence of the fast premixing. It was recognized that there were a substantial number of data points exhibiting residual fuel at intermediate temperatures (i.e., preheated to above-ignition point), indicating the existence of data points with a certain degree of incomplete combustion. Stoichiometric reactions at temperatures close to the adiabatic flame temperature were also observed, although such points were in the minority.

Although our single-shot multiscalar measurements were somewhat limited in being able to resolve only three of the major species, these three species and the temperature, nonetheless, are perhaps the most important scalars with regards to combustion simulation and modeling from the standpoint of fuel-oxidizer mixing and heat release. These scalar triplets provide direct correlations and PDFs which permit a unique visualization of the nature of the turbulent mixing and its impact on chemical reactions in a realistic

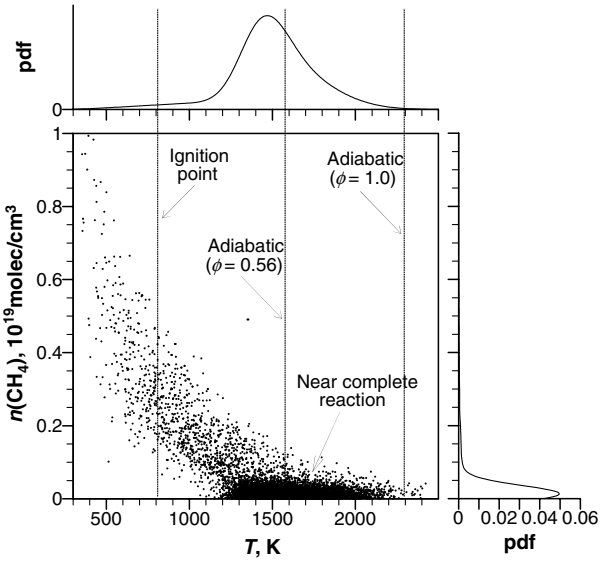

Fig. 12 Overall correlation between temperature and CH_4 number density, along with their PDFs.

flame at elevated pressure. We believe that the encouraging results from the present experiment not only provide insight to the fundamental aspects of the LDI combustion process, but affirm our choices in the design of the experimental apparatus and platform.

Acknowledgments

The authors acknowledge financial support by the Supersonics program and the Subsonic Fixed Wing program under Fundamental Aeronautics at NASA John H. Glenn Research Center at Lewis Field. The authors also acknowledge Gregg Calhoun for his assistance in the operation of the facilities.

References

[1] Grinstein, F. F., Liu, N.-S., and Oefelein, J. C., "Introduction: Combustion Modeling and Large Eddy Simulation: Development and Validation Needs for Gas Turbine," *AIAA Journal*, Vol. 44, No. 4, 2006, p. 673. doi:10.2514/1.23786

[2] Menon, S., and Patel, N., "Subgrid Modeling for Simulation of Spray Combustion in Large-Scale Combustors," *AIAA Journal*, Vol. 44, No. 4, 2006, pp. 709–723. doi:10.2514/1.14875

[3] Moin, P., and Apte, S. V., "Large-Eddy Simulation of Realistic Gas Turbine Combustors," *AIAA Journal*, Vol. 44, No. 4, 2006, pp. 698–708. doi:10.2514/1.14606

[4] Huang, Y., Wang, S., and Yang, Vigor, "Systematic Analysis of Lean-Premixed Swirl-Stabilized Combustion," *AIAA Journal*, Vol. 44, No. 4, 2006, pp. 724–740. doi:10.2514/1.15382

[5] Martin, C. E., Benoit, L. J.-L., Sommerer, Y., Nicoud, F., and Poinsot, T., "Large-Eddy Simulation and Acoustic Analysis of a Swirled Staged Turbulent Combustor," *AIAA Journal*, Vol. 44, No. 4, 2006, pp. 741–750. doi:10.2514/1.14689

[6] Geyer, D., Kempf, A., Dreizler, A., and Janicka, J., "Turbulent Opposed-Jet Flames: A Critical Benchmark Experiment for Combustion LES," *Combustion and Flame*, Vol. 143, No. 4, 2005, pp. 524–548. doi:10.1016/j.combustflame.2005.08.032

[7] Sidwell, T., Richards, G., Casleton, K., Straub, D., Maloney, D., Strakey, P., Ferguson, D., Beer, S., and Woodruf, S., "Optically Accessible Pressurized Research Combustor for Computational Fluid Dynamics Model Validation," *AIAA Journal*, Vol. 44, No. 3, 2006, pp. 434–443. doi:10.2514/1.15197

[8] Oefelein, J. C., Schefer, R. W., and Barlow, R. S., "Toward Validation of Large Eddy Simulation for Turbulent Combustion," *AIAA Journal*, Vol. 44, No. 3, 2006, pp. 418–433. doi:10.2514/1.16425

[9] Barlow, R. S., "Laser Diagnostics and Their Interplay with Computations to Understand Turbulent Combustion," *Proceedings of the Combustion Institute*, Vol. 31, No. 1, 2007, pp. 49–75. doi:10.1016/j.proci.2006.08.122

[10] Barlow, R. S., Dreizler, A., and Kempf, A., "Summary: Eighth International Workshop on Measurement and Computation of Turbulent Nonpremixed Flames," *TNF8 Workshop Proceedings*, Sandia National Laboratories, Heidelberg, Germany, Aug. 2006.

[11] Meier, W., Keck, O., Noll, B., Kunz, O., and Stricker, W., "Investigations in the TECFLAM Swirling Diffusion Flame: Laser Raman Measurements and CFD Calculations," *Applied Physics B (Lasers and Optics)*, Vol. 71, No. 5, 2000, pp. 725–731. doi:10.1007/s003400000436

[12] Weigand, P., Meier, W., Duan, X. R., Stricker, W., and Aigner, V., "Investigations of Swirl Flames in a Gas Turbine Model Combustor: 1. Flow Field, Structures, Temperature, and Species Distributions," *Combustion and Flame*, Vol. 144, No. 1, 2006, pp. 205–224. doi:10.1016/j.combustflame.2005.07.010

[13] Meier, W., Duan, X. R., and Weigand, P., "Investigations of Swirl Flames in a Gas Turbine Model Combustor: 2. Turbulence-Chemistry Interactions," *Combustion and Flame*, Vol. 144, No. 1, 2006, pp. 225–236. doi:10.1016/j.combustflame.2005.07.009

[14] Lucht, R. P., Roy, S., Meyer, T. R., and Gord, J. R., "Femtosecond Coherent Anti-Stokes Raman Scattering Measurement of Gas Temperatures from Frequency-Spread Dephasing of the Raman Coherence," *Applied Physics Letters*, Vol. 89, No. 25, 2006, p. 251112. doi:10.1063/1.2410237

[15] Roy, S., Meyer, T. R., Lucht, R. P., Afzelius, M., Bengtsson, P.-E., and Gord, J. R., "Dual-Pump Dual-Broadband Coherent Anti-Stokes Raman Scattering in Reacting Flows," *Optics Letters*, Vol. 29, No. 16, 2004, pp. 1843–1845. doi:10.1364/OL.29.001843

[16] Vestin, F., Afzelius, M., Brackmann, C., and Bengtsson, P.-E., "Dual-Broadband Rotational Cars Thermometry in the Product Gas of Hydrocarbon Flames," *Proceedings of the Combustion Institute*, Vol. 30, No. 1, 2005, pp. 1673–1680. doi:10.1016/j.proci.2004.08.043

[17] Vestin, F., Sedarskya, D., Collina, R., Aldéna, M., Linnea, M., and Bengtsson, P.-E., "Rotational Coherent Anti-Stokes Raman Spectroscopy (CARS) Applied to Thermometry in High-Pressure Hydrocarbon Flames," *Combustion and Flame*, Vol. 154, No. 1, 2008, pp. 143–152. doi:10.1016/j.combustflame.2007.10.014

[18] Weikl, M. C., Seeger, T., Hierold, R., and Leipertz, A., "Dual-Pump CARS Measurements of N2, H2 and CO in a Partially Premixed Flame, *Journal of Raman Spectroscopy*," Vol. 38, No. 8, 2007, pp. 983–988. doi:10.1002/jrs.1700

[19] Weikl, MC, Beyrau, F, and Leipertz, A, "Simultaneous Temperature and Exhaust-Gas Recirculation-Measurements in a Homogeneous Charge-Compression Ignition Engine by Use of Pure Rotational Coherent Anti-Stokes Raman Spectroscopy," *Applied Optics*, Vol. 45, No. 15, 2006, pp. 3646–3651. doi:10.1364/AO.45.003646

[20] Weikl, M. C., Beyrau, F., Kiefer, J., Seeger, T., and Leipertz, A., "Combined Coherent Anti-Stokes Raman Spectroscopy and Linear Raman Spectroscopy for Simultaneous Temperature and Multiple Species Measurements," *Optics Letters*, Vol. 31, No. 12, 2006, pp. 1908–1910. doi:10.1364/OL.31.001908

[21] Dibble, R. W., Masri, A. R., and Bilger, R. W., "The Spontaneous Raman Scattering Technique Applied to Nonpremixed Flames of Methane," *Combustion and Flame*, Vol. 67, No. 3, 1987, pp. 189–206. doi:10.1016/0010-2180(87)90095-2

[22] Nguyen, Q. V., Dibble, R. W., Carter, C. D., Fiechtner, G. J., and Barlow, R. S., "Raman-LIF Measurements of Temperature, Major Species, OH, and NO in a Methane-Air Bunsen Flame," *Combustion and Flame*, Vol. 105, No. 4, 1996, pp. 499–510. doi:10.1016/0010-2180(96)00226-X

[23] Hassel, E. P., and Linow, S., "Review Article: Laser Diagnostics for Studies of Turbulent Combustion," *Measurement Science and Technology*, Vol. 11, No. 2, 2000, pp. R37–R57. doi:10.1088/0957-0233/11/2/201

[24] Nooren, P. A., Versluis, M., van der Meer, T. H., Barlow, R. S., and Frank, J. H., "Raman-Rayleigh-LIF Measurements of Temperature and Species Concentrations in the Delft Piloted Turbulent Jet Diffusion Flame," *Applied Physics B (Lasers and Optics)*, Vol. 71, No. 1, 2000, pp. 95–111. doi:10.1007/s003400000278

[25] Mansour, M. S., and Chen, Y., "Line Raman, Rayleigh, and Laser-Induced Predissociation Fluorescence Technique for Combustion with a Tunable KrF Excimer Laser," *Applied Optics*, Vol. 35, No. 21, 1996, pp. 4252–4260.

[26] Roths, E. W., and Andresen, P., "Application of Tunable Excimer Lasers to Combustion Diagnostics: A Review," *Applied Optics*, Vol. 36, No. 18, 1997, pp. 3971–4033. doi:10.1364/AO.36.003971

[27] Barlow, R. S., and Miles, P. C., "A Shutter-Based Line-Imaging System for Single-Shot Raman Scattering Measurements of Gradients in Mixture Fraction," *Proceedings of the Combustion Institute*, Vol. 28, No. 1, 2000, pp. 269–277.

[28] Kojima, J., and Nguyen, Q., "Laser Pulse-Stretching with Multiple Optical Ring Cavities," *Applied Optics*, Vol. 41, No. 30, 2002, pp. 6360–6370.

[29] Gu, Y., Rothe, E. W., Reck, G. P., Locke, R. J., Anderson, R. C., Hicks, Y. R., and Nguyen, Q.-V., "One-Dimensional UV-Raman Imaging of a Jet-A-Fueled Aircraft Combustor in a High Temperature and Pressure Test Cell: A Feasibility Study," *Combustion Science and Technology*, Vol. 174, No. 10, 2002, pp. 199–215. doi:10.1080/00102200290021506

[30] Hicks, Y. R., Lockes, R. J., and Anderson, R. C., "Optical Measurement and Visualization in High-Pressure, High-Temperature, Aviation Gas Turbine Combustors," NASA TM 2000-210377, Sept. 2000.

[31] Wehr, L., Meier, W., Kutne, P., and Hassa, C., "Single-Pulse 1D Laser Raman Scattering Applied in a Gas Turbine Model Combustor at Elevated Pressure," *Proceedings of the Combustion Institute*, Vol. 31, No. 2, 2007, pp. 3099–3106. doi:10.1016/j.proci.2006.07.148

[32] Norris, A. T., and Liu, N.-S., "Turbulent Chemical Interaction Models in NCC: Comparison," NASA TM 2006-214417, Dec. 2006.

[33] Sankaran, R., and Im, H. G., "Dynamic Flammability Limits of Methane/Air Premixed Flames with Mixture Composition Fluctuations," *Proceedings of the Combustion Institute*, Vol. 29, No. 1, 2002, pp. 77–84. doi:10.1016/S1540-7489(02)80014-1

[34] Tacina, R., Wey, C., Laing, P., and Mansour, A., "A Low NOx Lean-Direct Injection, Multi Point Integrated Module Combustor Concept for Advanced Aircraft Gas Turbines," NASA TM 2002-211347, April 2002.

[35] Kojima, J., and Nguyen, Q.-V., "Strategy for Multiscalar Raman Diagnostics in High-Pressure Hydrogen Flames," *New Developments in Combustion Research*, edited by W. J. Carey, NOVA Science Publishers, New York, 2006, pp. 227–256.

[36] Kojima, J., and Nguyen, Q.-V., "Measurement and Simulation of Spontaneous Raman Scattering in High-Pressure Fuel-Rich H2–Air Flames," *Measurement Science and Technology*, Vol. 15, No. 3, 2004, pp. 565–580. doi:10.1088/0957-0233/15/3/009

[37] Fureby, C., Grinstein, F. F., Li, G., and Gutmark, E. J., "An Experimental and Computational Study of a Multi-Swirl Gas Turbine Combustor," *Proceedings of the Combustion Institute*, Vol. 31, No. 2, 2007, pp. 3107–3114. doi:10.1016/j.proci.2006.07.127

[38] Archer, S., and Gupta, A. K., "Effects of Swirl and Combustion on Flow Dynamics in Lean Direct Injection Gas Turbine Combustion," AIAA Paper 2003-1343, Jan. 2003.

[39] Cooper, C. S., Ravikrishna, R. V., and Laurendeau, N. M., "Comparison of Laser-Saturated, Laser-Induced, and Planar Laser-Induced Fluorescence Measurements of Nitric Oxide in a Lean Direct-Injection Spray Flame," *Applied Optics*, Vol. 37, No. 21, 1998, pp. 4823–4833. doi:10.1364/AO.37.004823

[40] Kojima, J., and Nguyen, Q.-V., "Single-Shot Rotational Raman Thermometry for Turbulent Flames Using a Low-Resolution Bandwidth Technique," *Measurement Science and Technology*, Vol. 19, No. 1, 2008, p. 015406. doi:10.1088/0957-0233/19/1/015406.

[41] Kojima, J., and Nguyen, Q.-V., "Quantitative Analysis on Spectral Interference of Spontaneous Raman Scattering in High-Pressure Fuel-Rich Hydrogen-Air Flames," *Journal of Quantitative Spectroscopy and Radiative Transfer*, Vol. 94, No. 3, 2005, pp. 439–466. doi:10.1016/j.jqsrt.2004.10.004

[42] Meier, W., and Keck, O., "Laser Raman Scattering in Fuel-Rich Flames: Background Levels at Different Excitation Wavelengths," *Measurement Science and Technology*, Vol. 13, No. 5 2002, pp. 741–749. doi:10.1088/0957-0233/13/5/312

[43] Grünefeld, G., Beushausen, V. S., and Andresen, P. S., "Interference-Free UV-Laser-Induced Raman and Rayleigh Measurements in Hydrocarbon Combustion Using Polarization Properties," *Applied Physics B (Lasers and Optics)*, Vol. 61, No. 5, 1995, pp. 473–478. doi:10.1007/BF01081276

[44] Karpetis, A. N., and Gomez, A., "Temperature Measurements in Spray Flames by Spontaneous Raman Scattering," *Optics Letters*, Vol. 21, No. 10, 1996, pp. 704–706.

[45] Nguyen, Q.-V., "High-Speed Electromechanical Shutter for Imaging Spectrographs," U.S. Patent No. 6,937,331, filed Aug. 2005.

[46] Syred, N., "A Review of Oscillation Mechanisms and the Role of the Precessing Vortex Core (PVC) in Swirl Combustion Systems," *Progress in Energy and Combustion Science*, Vol. 32, No. 2, 2006, pp. 93–161. doi:10.1016/j.pecs.2005.10.002

[47] Grinstein, F. F., Young, T. R., Gutmark, E. J., Li, G., Hsiao, G., and Mongia, H. C., "Flow Dynamics in a Swirl Combustor," *Journal of Turbulence*, Vol. 3, No. 30, July 2002, p. 1. doi:10.1088/1468-5248/3/1/030

[48] Archer, S., and Gupta, A. K., "Effect of Swirl and Combustion on Flow Dynamics in Lean Direct Injection Gas Turbine Combustion," AIAA Paper 2003-1343, Jan. 2003.

[49] Peter, N., "Laminar Diffusion Flamelet Models in Nonpremixed Turbulent Combustion," *Progress in Energy and Combustion Science*, Vol. 10, No. 3, 1984, pp. 319–339. doi:10.1016/0360-1285(84)90114-X

[50] Williams, B. A., "Sensitivity of Calculated Extinction Strain Rate to Molecular Transport Formulation in Nonpremixed Counterflow Flames," *Combustion and Flame*, Vol. 124, No. 1, 2001, pp. 330–333. doi:10.1016/S0010-2180(00)00197-8

[51] Kim, S.-K., Yu, Y., Ahn, J., and Kim, Y.-M., "Numerical Investigation of the Autoignition of Turbulent Gaseous Jets in a High-Pressure Environment Using the Multiple-RIF Model," *Fuel*, Vol. 83, No. 3, 2004, pp. 375–386. doi:10.1016/j.fuel.2003.01.001

[52] Iannetti, A. C., and Chen, K. H., "Initial Comparison of National Combustion Code Simulations to Experimental Gas Turbine Combustor Data Using Various Chemistry Modules," AIAA Paper 2000-0330, Jan. 2000.

R. Lucht
Associate Editor